Supplement Information

Glucose-mediated independent pyrolysis strategy optimises the pore structure of MOF-derived carbon catalysts to promote the conversion of HMF to FDCA

Hao Peng,[+a] Zhan Chen,[+a] Peng Wang,[a] Haoyue Ma,[a] Song Zhang,[a] Shuai Li,[a] Ye Yuan,[a] Cheng Chen,[*a,b] Somboon Chaemchuen,[a] Soon Hyeok Hong,[*c] Zongkui Kou,[*a,b]

[a] State Key Laboratory of Advanced Technology for Materials Synthesis and Processing, Wuhan University of Technology, Wuhan 430070, P. R. China.

[b] Sanya Science and Education Innovation Park of Wuhan University of Technology, Sanya 572000, China.

[c] Department of Chemistry, Korea Advanced Institute of Science and Technology (KAIST), Daejeon 34141, Republic of Korea.

[+] These authors contributed equally to this work.

Corresponding Authors

*E-mail for Cheng Chen: chengchen@whut.edu.cn; *E-mail for Soon Hyeok Hong: soonhyeok.hong@kaist.ac.kr; *E-mail for Dr. Zongkui Kou: zongkuikou@whut.edu.cn.

Contents:

1. **Definition of Parameter Z**

The components of parameter Z, namely Smic, Stotal, Vmic, and Vtotal, represent micropore area, total specific surface area, micropore volume, and total pore volume, respectively. These parameters are directly measured through nitrogen physisorption experiments, and the test materials are primarily microporous in nature.

Typically, for gas or small molecule transformation reactions, microporous structures are well-suited to meet the demands for adsorption and diffusion during the reaction process. An increase in micropores typically leads to a larger specific surface area, and thus, there is often a positive correlation between micropore surface area and catalytic performance[1-3]. This suggests that the pore structure's role in adsorption and mass transfer during the reaction is frequently treated as a unified factor. In this process, we applied a one-sided fitting method (Figures S4 and S5), but the results were not ideal. This indirectly confirms the complexity of multi-step reactions and indicates that two sets of parameters are required to address this issue, thereby improving the accuracy of Z in describing the catalyst's transport properties.

In this case, the intermediate HMFCA exhibits poor affinity for the microporous material, as confirmed by in situ infrared analysis (see Fig S9). In situ DRIFTS shows that CuC-$GLU_{0.2}$ exhibits adsorption-related new bands earlier, indicating that its pore architecture provides better accessibility and mass transport for HMFCA, thereby promoting its subsequent conversion to FDCA. Therefore, it is necessary to reconsider the role of pore structure in multi-step reactions, particularly the potential competitive effects between different pore structures. We believe that the proportion of pore types is a crucial factor influencing the reaction process. Hence, refining parameter Z into two components, namely $1/(S_{mic}/S_{total})$ and $1/(V_{mic}/V_{total})$, would represent the competitive adsorption and diffusion capacities of mesopores within materials containing multiple pore types in the catalyst.

2. Supplementary results

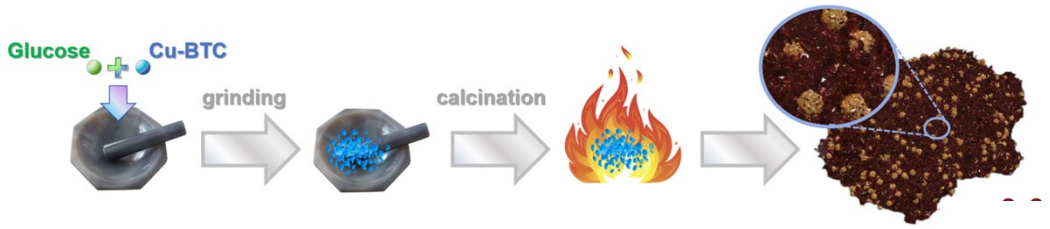

Figure S1. Synthesis of CuC-GLU$_x$ (x= 0.0-0.5, and the prepared material without glucose was marked as CuC-GLU$_{0.0}$.

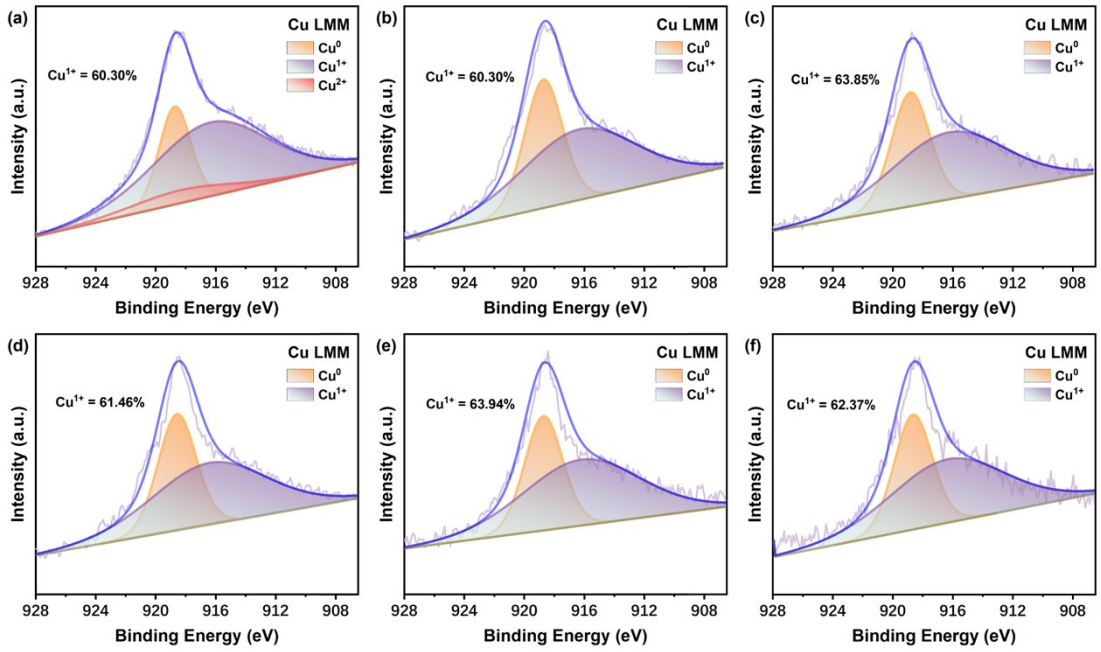

Figure S2. Cu LMM spectra of (a) CuC-GLU$_{0.0}$, (b) CuC-GLU$_{0.1}$, (c) CuC-GLU$_{0.2}$, (d) CuC-GLU$_{0.3}$, (e) CuC-GLU$_{0.4}$, (f) CuC-GLU$_{0.5}$.

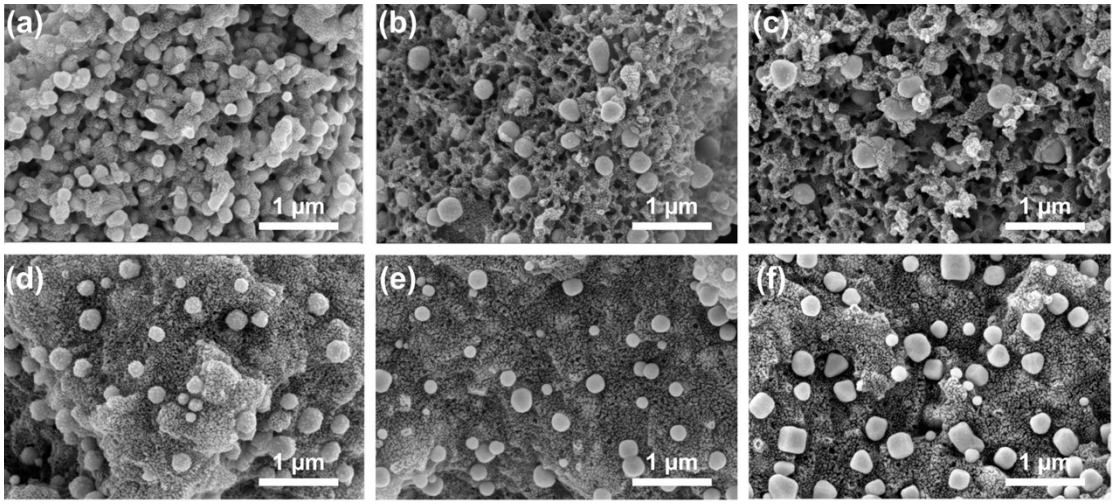

Figure S3. SEM images of (a) CuC-$GLU_{0.0}$, (b) CuC-$GLU_{0.1}$, (c) CuC-$GLU_{0.2}$, (d) CuC-$GLU_{0.3}$ (e) CuC-$GLU_{0.4}$ (f) CuC-$GLU_{0.5}$.

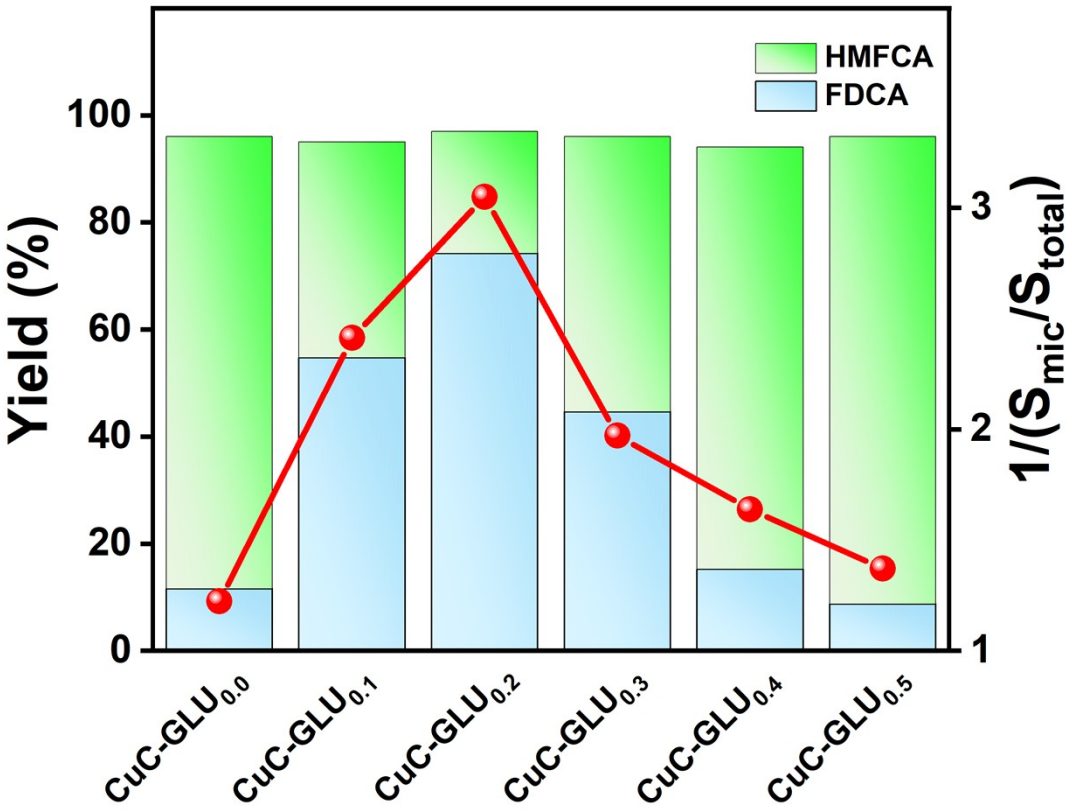

Figure S4. Catalytic performance and $1/(S_{mic}/S_{total})$ of CuC-GLU_x.

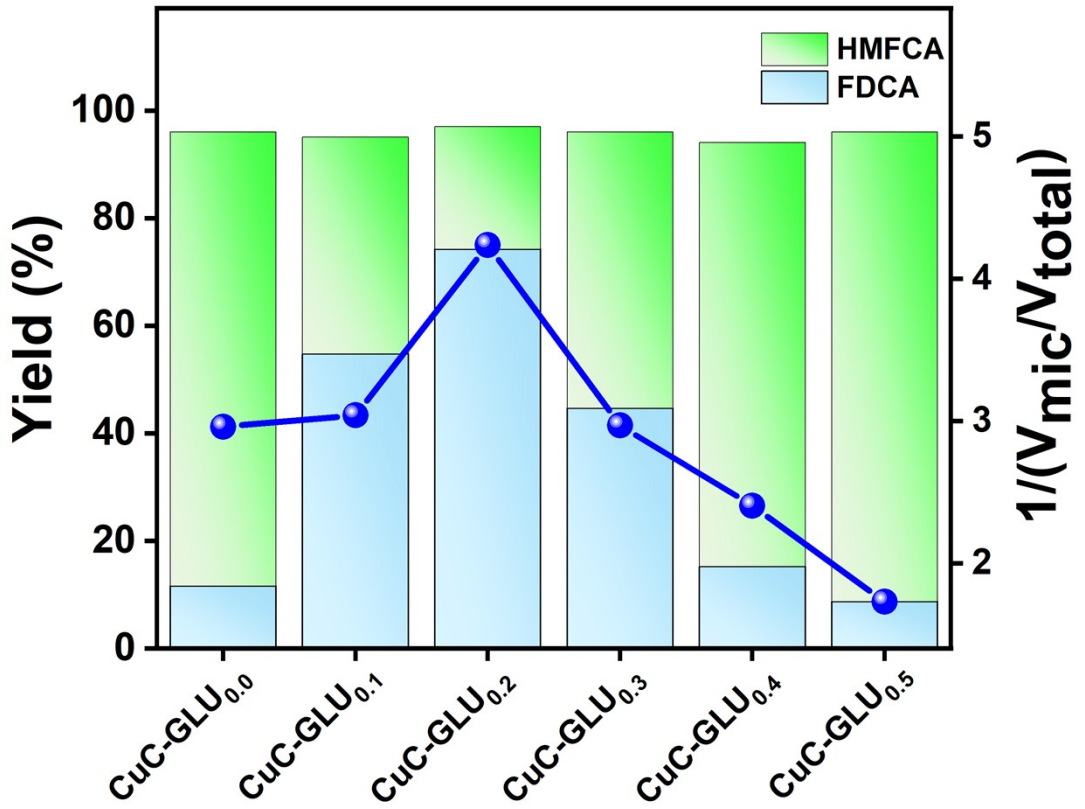

Figure S5. Catalytic performance and $1/(V_{mic}/V_{total})$ of CuC-GLU_x.

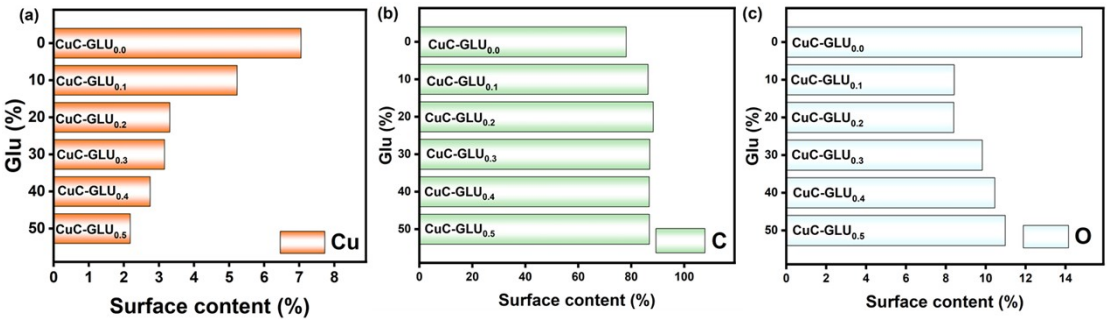

Figure S6. Surface element content of CuC-GLU$_x$: (a) Cu, (b) C and (c) O.

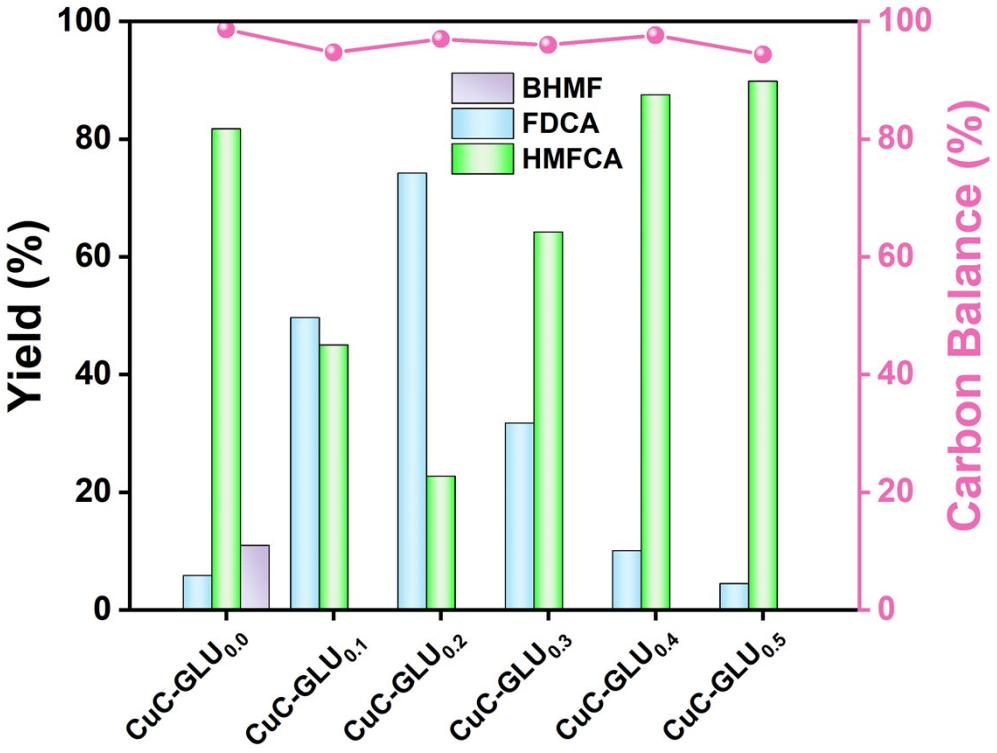

Figure S7. performance of CuC-GLU_x after dosage correction (using CuC-$GLU_{0.2}$ as a reference). The dose of catalyst was corrected to *m* mg and the rest of the conditions were the same as for the general process.

Corrective methods:

$A = |S_{total}| \cdot |Cu(_{Surface\ content})|$

$A_{min} = A_{(CuC\text{-}GLU_{0.2})} = 629.07$

$m = 100(A_{min})/|S_{total}| \cdot |Cu(_{Surface\ content})|$ mg

Table S1. Valence state content and catalytic performance of CuC-GLU_x.

Samples	Mole ratio of Cu^0/Cu	Mole ratio of Cu^+/Cu	Mole ratio of Cu^{2+}/Cu	HMF Conversion (%)	Selectivity (%)	
					FDCA	HMFCA
$CuC\text{-}GLU_{0.0}$[a]	23.55	60.30	16.15	100	11.58	84.45
$CuC\text{-}GLU_{0.1}$[a]	39.70	60.30	0	100	54.72	40.32
$CuC\text{-}GLU_{0.2}$[a]	36.15	63.85	0	100	74.22	22.77
$CuC\text{-}GLU_{0.3}$[a]	38.54	61.46	0	100	44.62	51.41
$CuC\text{-}GLU_{0.4}$[a]	36.06	63.94	0	100	15.20	78.85
$CuC\text{-}GLU_{0.5}$[a]	37.63	62.37	0	100	8.73	87.30
$CuC\text{-}GLU_{0.2}$[b]	36.15	63.85	0	100	55.07	40.01
$R\text{-}CuC\text{-}GLU_{0.2}$[b]	25.63	60.41	13.96	84.33	3.17	24.64
$RA\text{-}CuC\text{-}GLU_{0.2}$[b]	37.14	62.86	0	100	49.13	44.77

[a] The reaction conditions consisted of HMF (32 mg, 0.25 mmol), catalyst (100 mg), NaOH (22 mg, 0.55 mmol), 0.75 mL water, maintained at 100 °C for 18 h unless otherwise noted. [b] 12 h instead of 18 h.

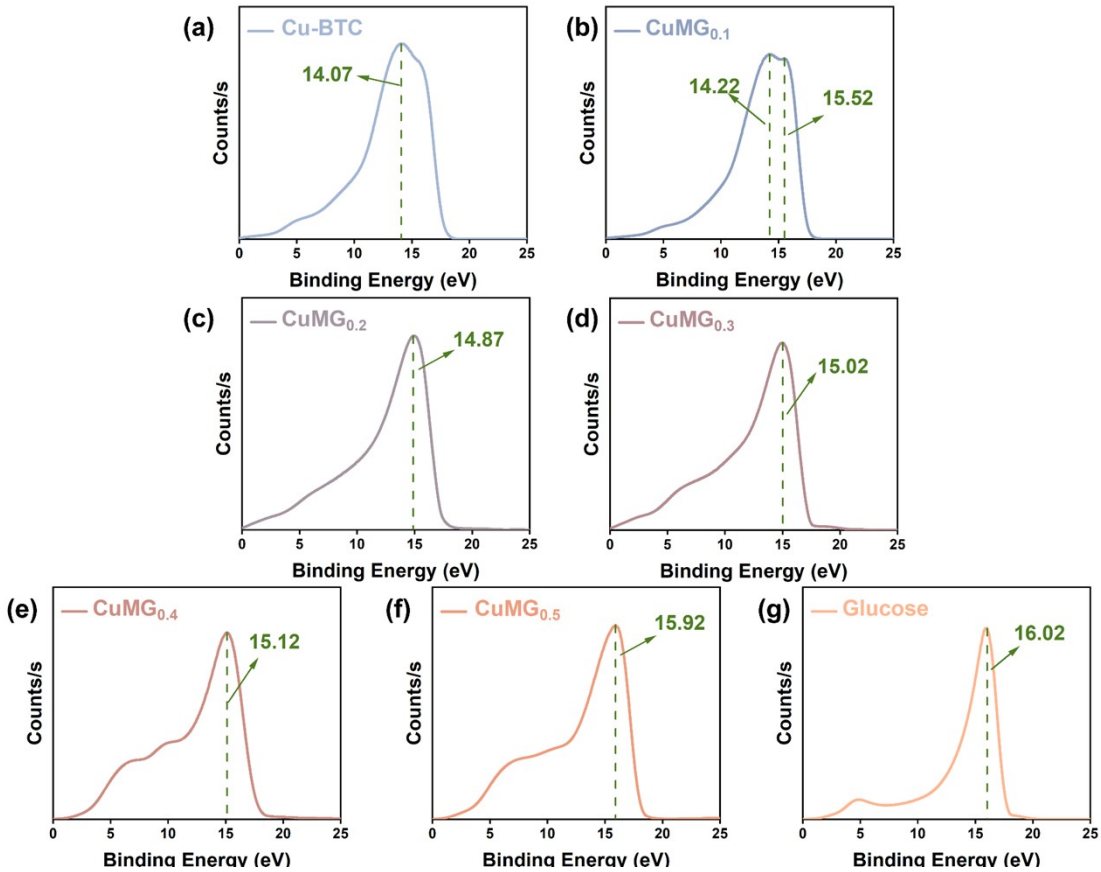

Figure S8. UPS spectra of (a) Cu-BTC, (b) $CuMG_{0.1}$, (c) $CuMG_{0.2}$, (d) $CuMG_{0.3}$, (e) $CuMG_{0.4}$, (f) $CuMG_{0.5}$, (g) Glucose.

Table S2. Catalytic performance of CuC-$GLU_{0.2}$ for HMFCA at different concentrations

Samples	HMF (mmol)	HMFCA (mmol)	Yield (%)	
			FDCA	HMFCA
CuC-$GLU_{0.2}$	0.125	0.125	50.81	44.42
CuC-$GLU_{0.2}$	0	0.25	54.18	43.67
CuC-$GLU_{0.2}$	0	0.5	24.82	73.14
CuC-$GLU_{0.2}$	0	0.75	17.12	80.24
CuC-$GLU_{0.2}$	0	1.00	11.50	87.13

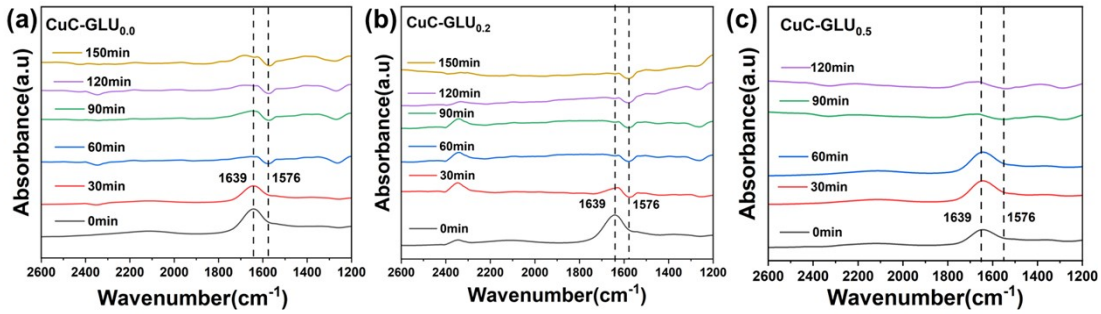

Figure S9. In Situ DRIFTS spectrum of HMFCA oxidation catalyzed by (a) CuC-$GLU_{0.0}$, (b) CuC-$GLU_{0.2}$, (c) CuC-$GLU_{0.5}$.

Table S3. Catalytic performance of catalysts with different particle sizes

Samples	Average particle size（nm）	Yield (%)		HMF Conversion (%)
		FDCA	HMFCA	
$CuC\text{-}GLU_{0.0}$	221.51	11.58	84.45	100
$CuC\text{-}GLU_{0.1}$	213.35	54.72	40.32	100
$CuC\text{-}GLU_{0.2}$	181.25	74.22	22.77	100
$CuC\text{-}GLU_{0.3}$	210.47	44.62	51.41	100
$CuC\text{-}GLU_{0.4}$	204.54	15.20	78.85	100
$CuC\text{-}GLU_{0.5}$	260.27	8.73	87.30	100

The reaction conditions consisted of HMF (32 mg, 0.25 mmol), catalyst (100 mg), NaOH (22 mg, 0.55 mmol), 0.75 mL water, maintained at 100 °C for 18 h unless otherwise noted.

Table S4. Comparison of the present work with representative catalytic systems reported in the literature.

Catalyst	Solvent	Base	Temperature	Oxidising agents	Selectivity	FDCA Yield	Recycle	Reference
CuC-$GLU_{0.2}$	H_2O	NaOH	100	Air (1bar)	100	74.22	11	This work
CuCl	MeCN	-	RT	*t*-BuOOH	100	50	-	4
Co-Cu-CN	H_2O	Na_2CO_3	100	O_2 (10 bar)	99	95	5	5
a-Co/Cu-NC		Na_2CO_3	90 °C	O_2 (40 mL min^{-1})	100	>99	5	6
Mn@NC	H_2O	NaOH NaClO	Rt	Air (1 bar)	100	94	5	7
Co-SACs	H_2O	-	65	O_2 (3 bar)	100	99.2	6	8
CoMn/N@C	H_2O	Cs_2CO_3	85	O_2 (1 bar)	100	96	6	9
MnO_2	H_2O	$NaHCO_3$	110	O_2 (5 bar)	100	96.7	6	10
$Mn_8Fe_3O_x$	DMSO	-	70	TBHP, air (1bar)	100	76.9	5	11
Ru/Fe-NC	H_2O	-	130	O_2 (1 Mpa)	100	98.6	6	12
Pt-Cu/AC	H_2O	-	150	O_2 (1 Mpa)	100	99	3	13
Pt-Pd	H_2O	-	100	O_2 (10 bar)	100	99	6	14

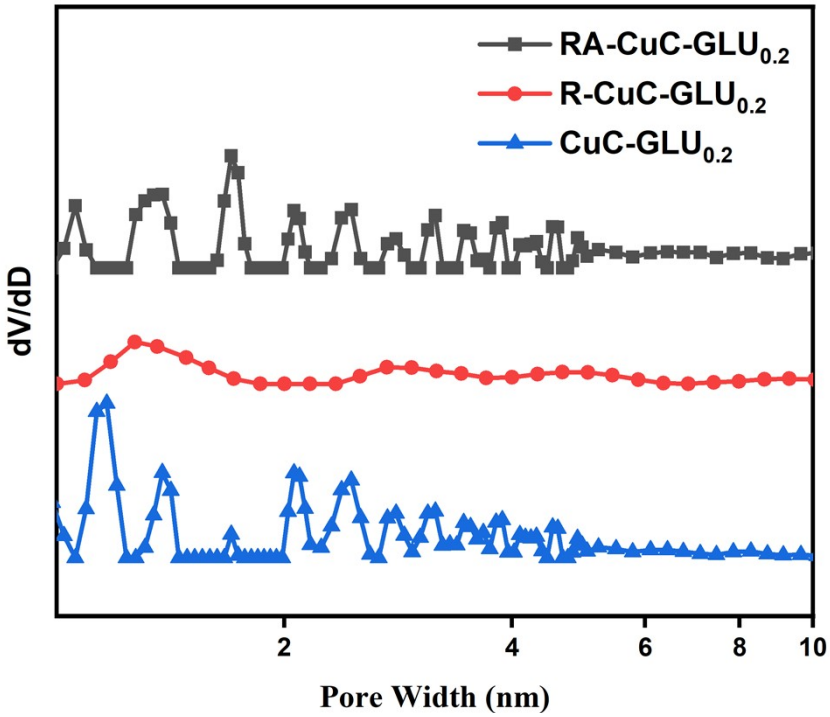

Figure S10. Pore size distribution of CuC-GLU_{02}, R-CuC-$GLU_{0.2}$ and RA-CuC-$GLU_{0.2}$.

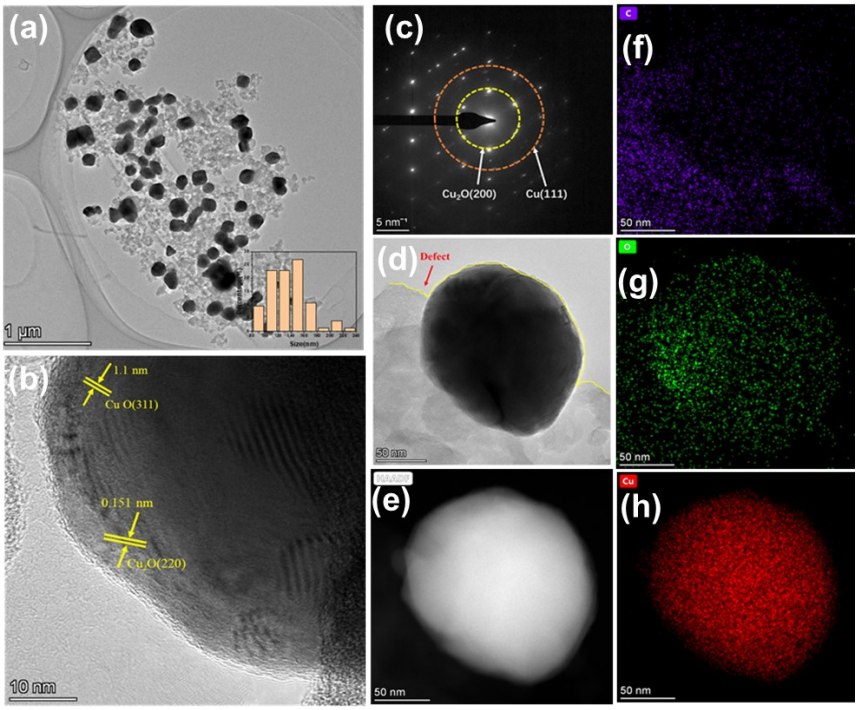

Figure S11. (a) TEM images, (b) HRTEM images, (c) SAED images, (d-h) EDS elemental mapping images of CuC-$GLU_{0.2}$

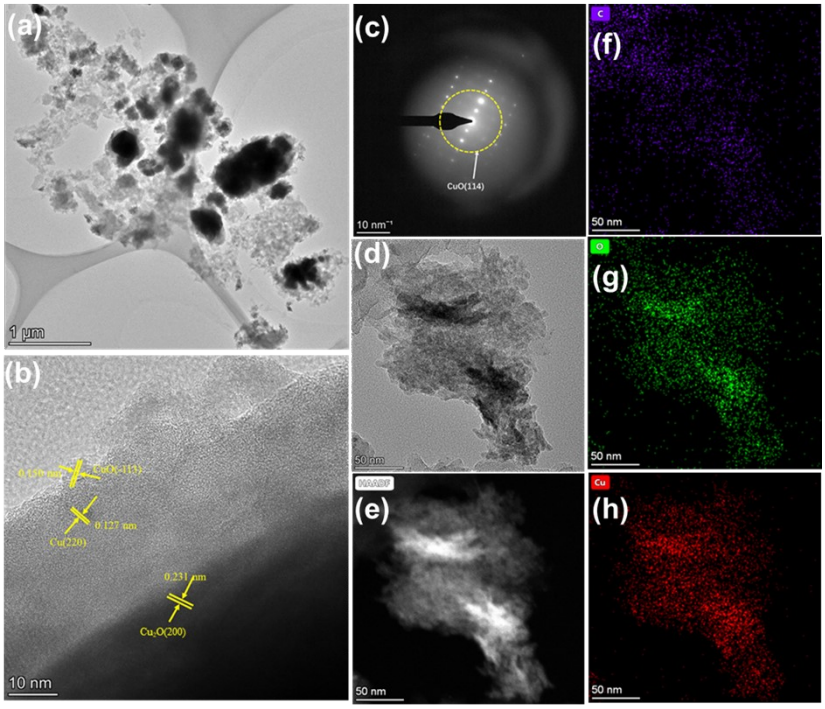

Figure S12. (a) TEM images, (b) HRTEM images, (c) SAED images, (d-h) EDS elemental mapping images of R-CuC-$GLU_{0.2}$

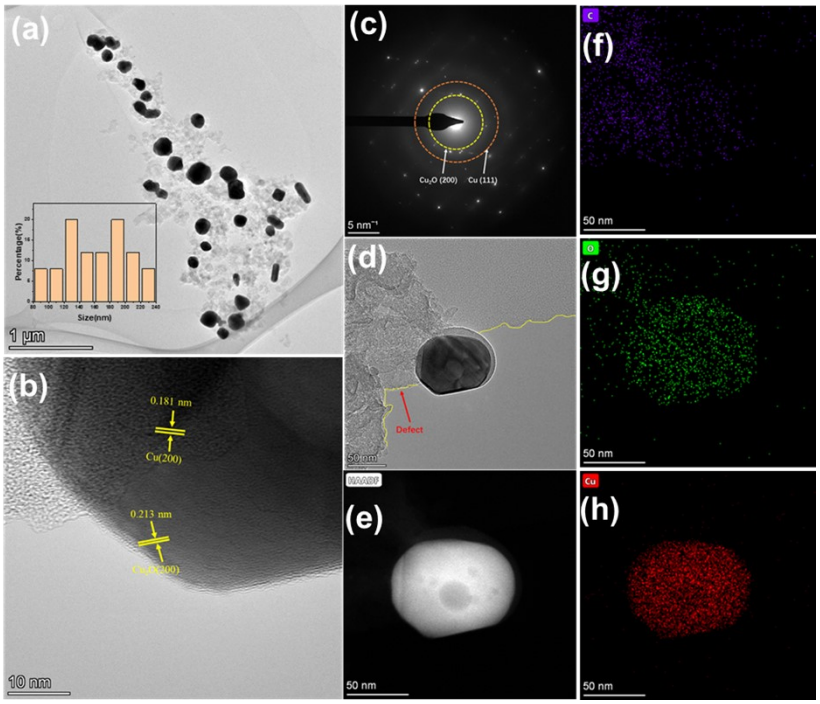

Figure S13. (a) TEM images, (b) HRTEM images, (c) SAED images, (d-h) EDS elemental mapping images of RA-CuC-$GLU_{0.2}$

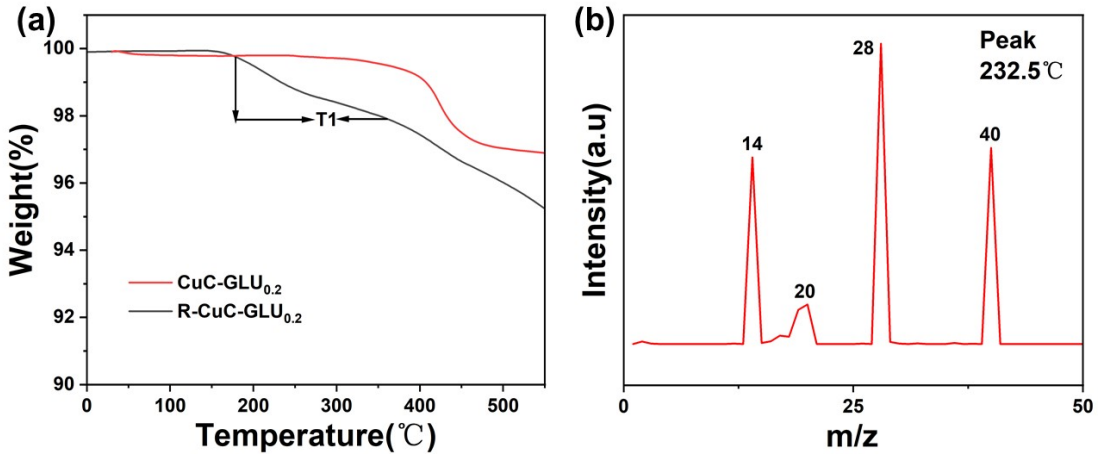

Figure S14. (a) The TG curve of CuC-$GLU_{0.2}$ and R-CuC-$GLU_{0.2}$, (b) The TGA-MS curve of R-CuC-$GLU_{0.2}$.

Table S5. Structural parameters of CuC-GLU_x.

Samples	pore size/nm	$S_{total}/m^2 \cdot g^{-1}$	S_{mic}/S_{total}[a]	$V_{mic}/cm^3 \cdot g^{-1}$	V_{mic}/V_{total}[b]
CuC-$GLU_{0.2}$	11.36	190.05	0.3279	0.027	0.2347
R-CuC-$GLU_{0.2}$	5.91	76.4591	0.6531	0.9827	0.5871
RA-CuC-$GLU_{0.2}$	10.32	220.01	0.3953	0.032	0.2471

3. Characterization data for the furan-based compounds

5-Hydroxymethylfurfural (HMF). ^{1}H NMR (500 MHz, D_2O) δ 9.34 (s, 1H), 7.41 (s, 1H), 6.58 (s, 1H), 4.64-4.57 (m, 2H). ^{13}C NMR (126 MHz, D_2O) δ 180.2, 161.6, 151.8, 126.7, 110.9, 56.2.

5-Hydroxymethyl-2-furancarboxylic acid (HMFCA). ^{1}H NMR (500 MHz, D_2O) δ 6.92 (s, 1H), 6.39 (s, 1H), 4.55-4.50 (m, 2H). ^{13}C NMR (126 MHz, D_2O) δ 166.7, 157.7, 148.8, 116.0, 115.8, 109.3, 109.1, 56.4. (Note: the NMR data are based on the sodium salt of HMFCA).

2,5-Furandicarboxylic acid (FDCA). ^{1}H NMR (500 MHz, D_2O) δ 7.00 (s, 1H). ^{13}C NMR (126 MHz, D_2O) δ 166.2, 150.3, 115.8, 115.7. (Note: the NMR data are based on the sodium salt of FDCA).

2,5-Dihydroxymethylfuran (BHMF). ^{1}H NMR (500 MHz, D_2O) δ 6.36 (s, 2H), 4.58-4.52 (m, 4H). ^{13}C NMR (126 MHz, D_2O) δ 153.8, 109.1, 56.0.

Original ^{1}H and ^{13}C NMR spectra for the furan-based compounds

- ^{1}H NMR spectrum for HMF

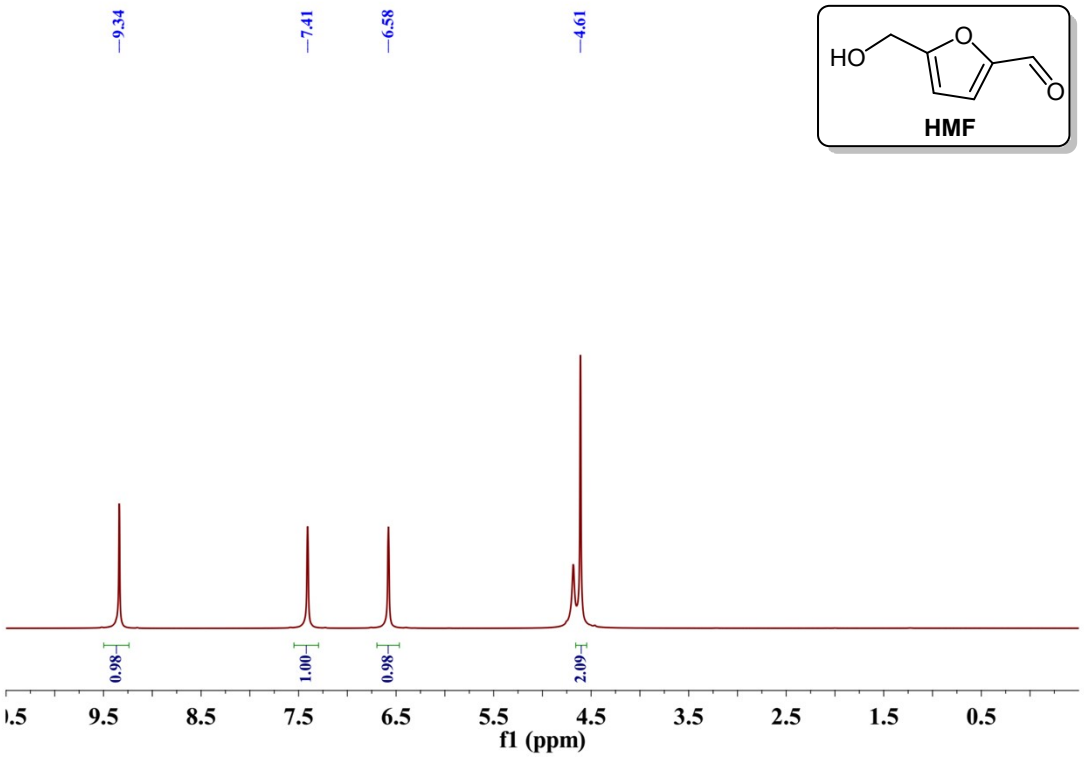

- ^{13}C NMR spectrum for HMF

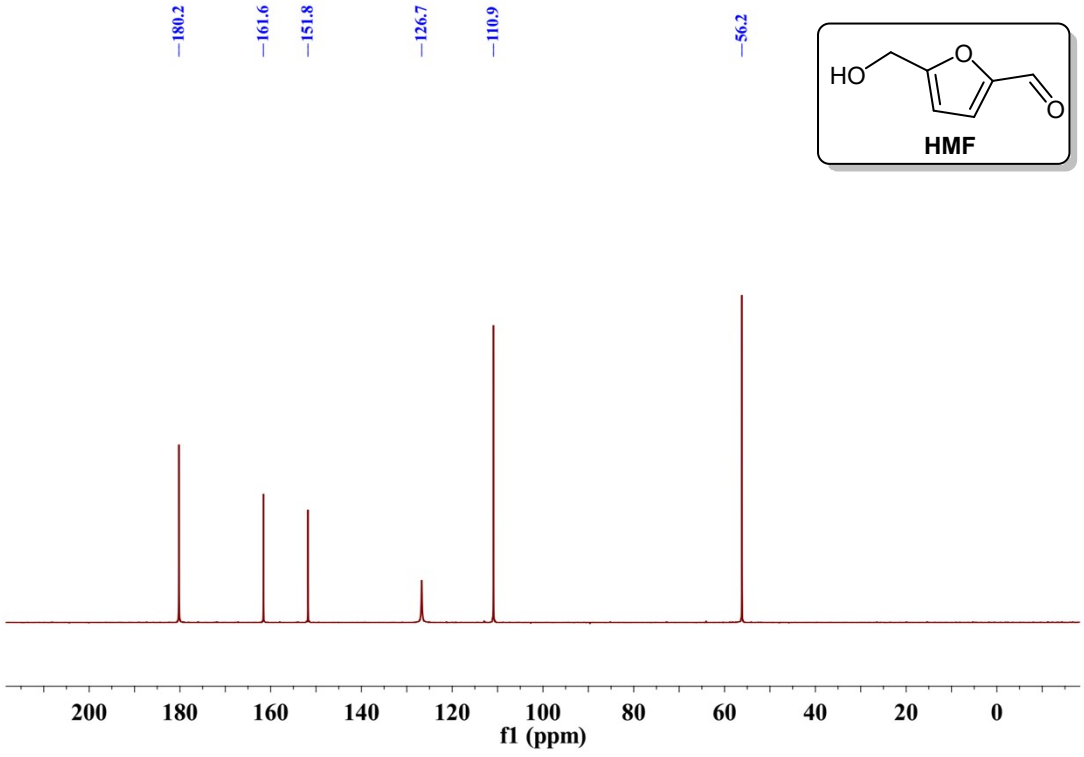

➢ ^{1}H NMR spectrum for HMFCA (sodium salt)

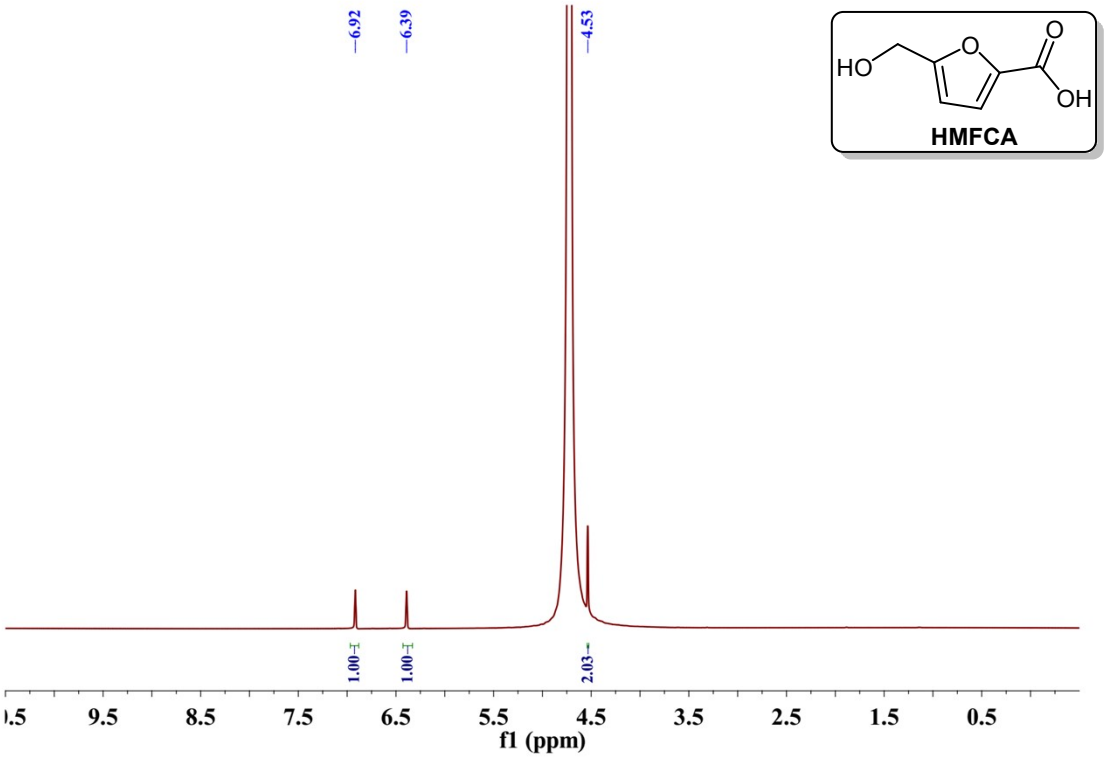

➢ ^{13}C NMR spectrum for HMFCA (sodium salt)

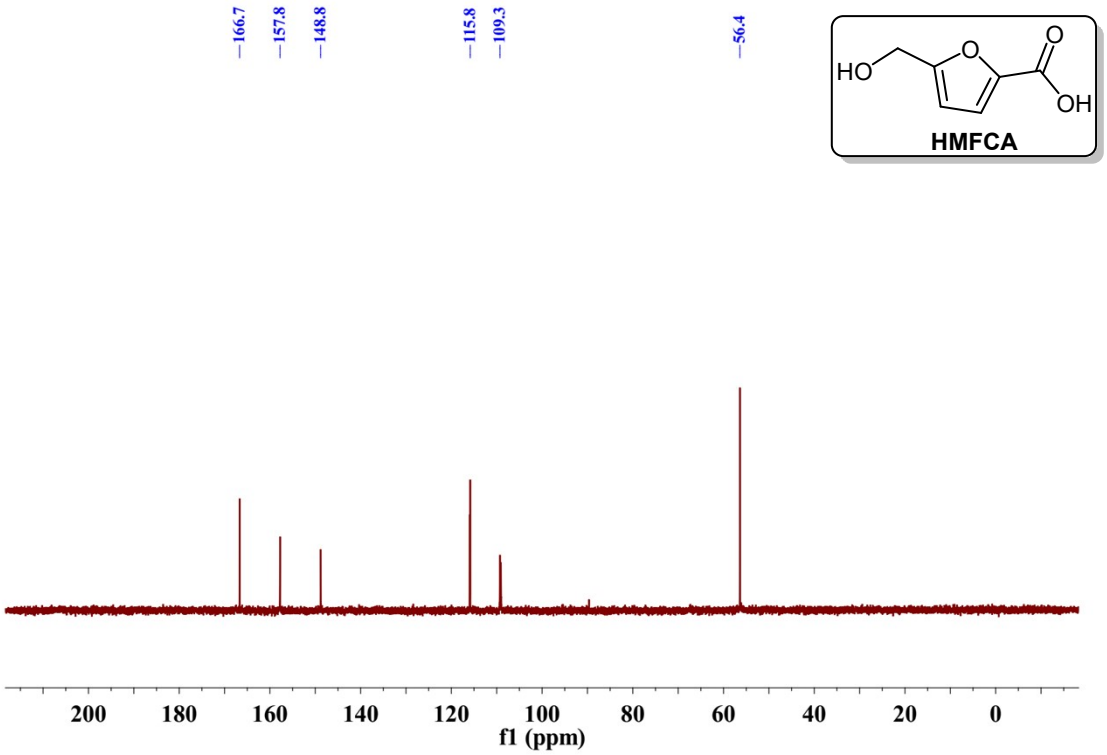

➢ ^{1}H NMR spectrum for FDCA (sodium salt)

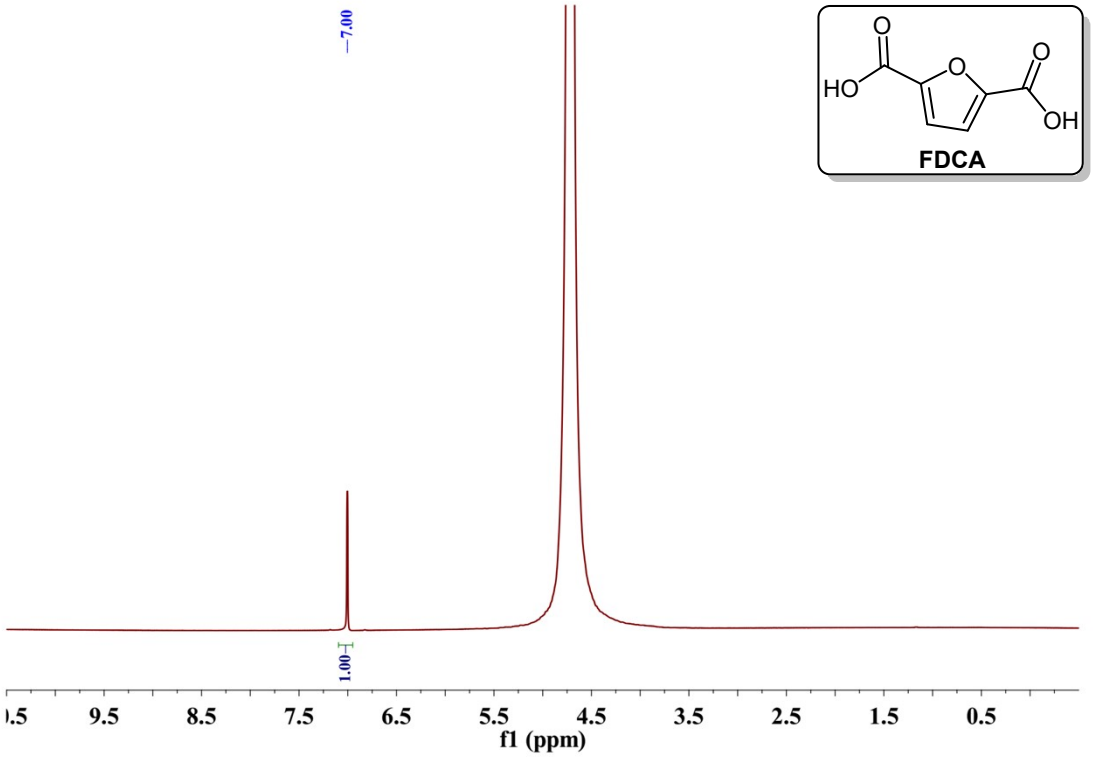

➢ ^{13}C NMR spectrum for FDCA (sodium salt)

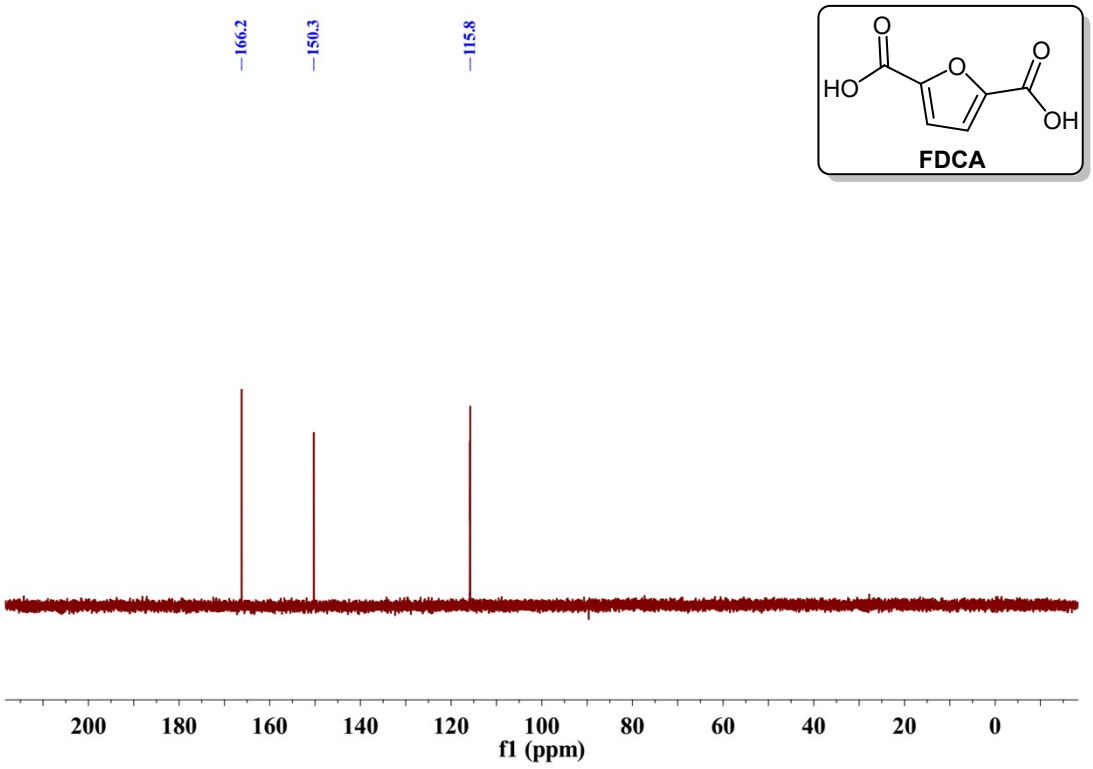

➢ ^{1}H NMR spectrum for BHMF

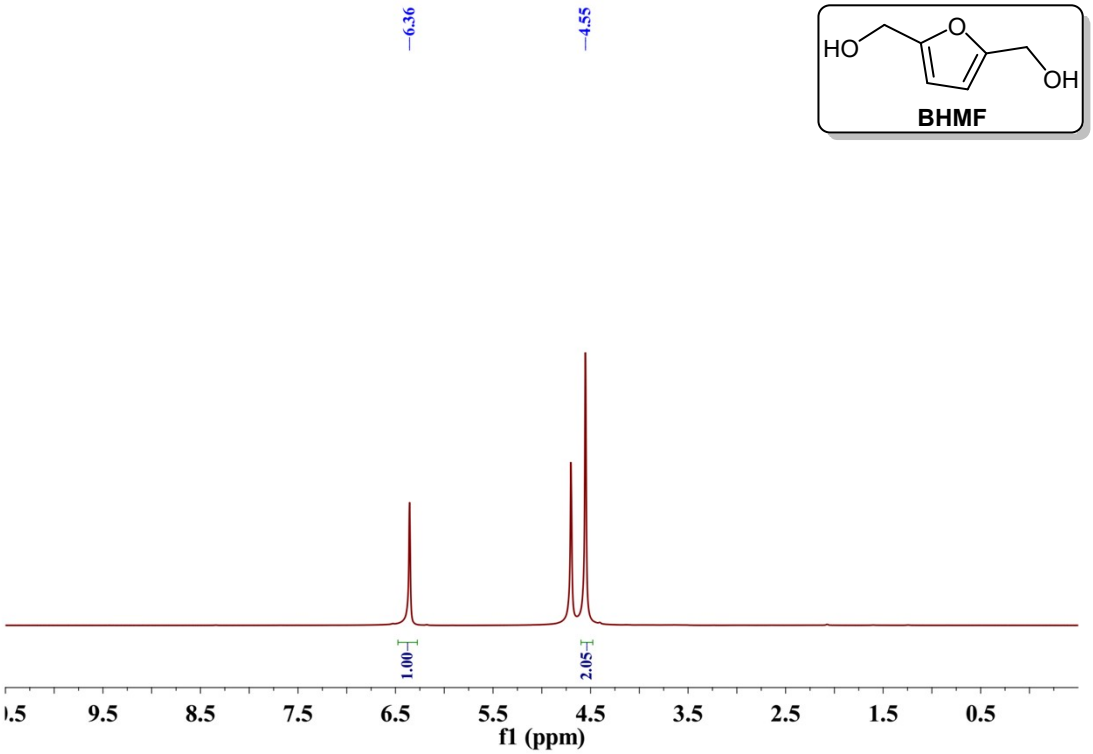

➢ ^{13}C NMR spectrum for BHMF

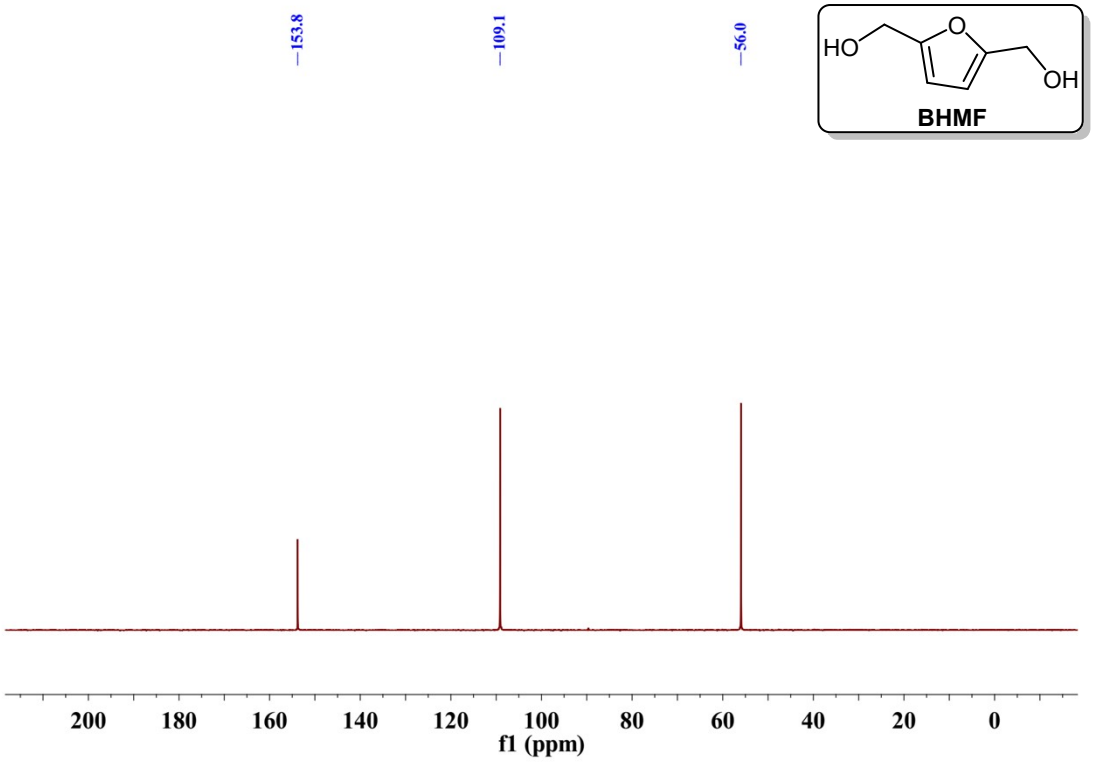

➢ ^{1}H NMR of selected reaction mixture

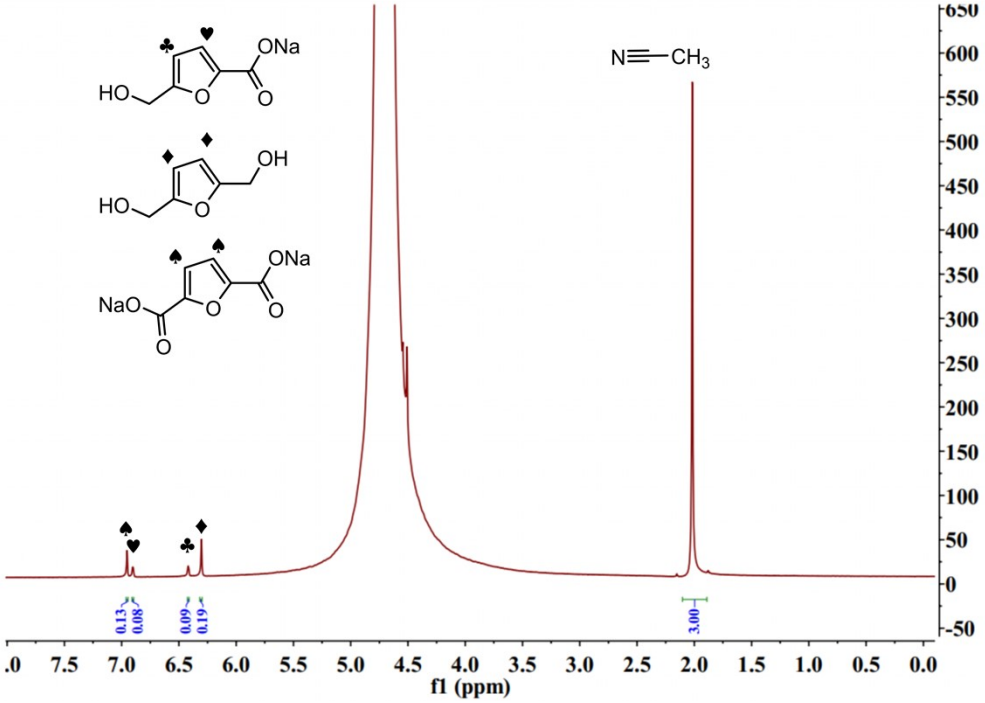

The mixture was obtained under the reaction conditions of HMF (32 mg, 0.25 mmol), CuC-$GLU_{0.2}$ (100 mg), NaOH (22 mg, 0.55 mmol), 1.5 mL water, 100 °C, 18 h (Fig. 3). All products were calculated based on the precise amount of acetonitrile (41 mg, 1.00 mmol) used:

Yield $_{(BHMF)}$ = 2(∫ ♦ /∫ acetonitrile) %

Yield $_{(HMFCA)}$ = 2(∫ ❤ /∫ acetonitrile) %

Yield $_{(FDCA)}$ = 2(∫ ♠ /∫ acetonitrile) %

Carbon Balance = Yield $_{(FDCA)}$ +Yield $_{(HMFCA)}$ + Yield $_{(BHMF)}$

Reference

1. S. Dahle, J. Meuthen, W. Viöl, W. M. Friedrichs, *Appl. Surf. Sci.*, 2013, **284**, 514–522.

2. H. Chen, L. Wang, J. Yang, R.T. Yang, *J. Phys. Chem. C.*, 2013, **117**, 7565–7576.

3. K.T.V. Rao, Y. Hu, Z. Yuan, Y. Zhang, C. Xu, *Chem. Eng. J.*, 2021, **404**, 127063.

4. T. S. Hansen, I. Sádaba, E. J. García, A. Riisager. *Appl. Catal. A*., 2013, **456**, 44–50.

5. T. Jing, S. Yang, Y. Feng, T. Li, Y. Zuo, D. Rao, *Nano Res.,* 2023, **16**, 6670−6678

6. T. Jing, S. Yang, T. Li, Y. Wan, H. Jia, Y. Feng, Y. Zuo, D. Rao, *Adv. Funct. Mater*, 2024, **34**, 2407335.

7. P. Wang, P, J. F. Gu, Z. Chen, H. Y. Ma, X. C. Li, S. Li, *Eur. J. Inorg. Chem.*, 2025, **28**, e202400642.

8. J. Li, G. Wang, W. Sui, A. M. Parvez, T. Xu, C. Si, J. Hu, *Adv. Colloid Interface Sci.,* 2024, **329**, 103176.

9. H. Zhou H. Xu, Y. Liu, *Appl. Catal. B, 2019,* **244**, 965−973.

10. B. Liu, H. Liu, S. Sun, Z. Ma, Y. Zhang, R. Nie, J. Fu, *Adv. Funct. Mater*., 2025, **35**, 2504172.

11. H. Lu, J. Bai, F. Yan, X. Zhang, Y. Jin, J. Wang, P. Chen, M. Zhou, *J. Fuel Chem. Technol.,* 2021, **49**, 312−321.

12. H. Liu, J. Zhang, X. Li, R. Zhang, W. Jia, J. Zhang, Y. Sun, L. Peng, *Appl. Catal. B,* 2025, **365**, 12499.

13. X. Cheng, S. Li, S. Liu, Y. Xin, J. Yang, B. Chen and H. Liu, *Chem. Commun.*, 2022, **58**, 1183−1186.

14. X. Zhong, Y. Wei, S. Sadjadi, D. Liu, M. Li, T. Yu, G. Zhuang, P. Yuan, *Appl. Clay Sci.,* 2022, **226**, 106574.